Proceedings of the 9th World Congress on Momentum, Heat and Mass Transfer (MHMT 2024)
London, United Kingdom – April 11 – 13, 2024
Paper No. ICMFHT 138
DOI: 10.11159/icmfht24.138

Numerical Model of High-Intensity Focused Applied to Soft Tissues

Paolo Guida, William L. Roberts
[1]King Abdullah University of Science and Technology (KAUST)
Thuwal, 23955, Saudi Arabia
paolo.guida@kaust.edu.sa; william.roberts@kaust.edu.sa

Abstract - High-Intensity Focused Ultrasounds (HIFU) technology has several applications in the medical field, such as tumour ablation and drug delivery. HIFU technology uses ultrasound to induce temperature increase and, eventually, cavitation in each location to destroy a particular tissue or activate a given drug. One of the limitations of HIFU is the side damage caused because of the inaccuracy given by the very complex composition of the human body. Computational fluid dynamics analysis can help evaluate the size of the cavitation zone that forms at the focal point and estimate eventual deviation from the expected location. The numerical simulation can also help estimate the temperatures reached at the focal point or design new devices.
The numerical model proposed to simulate HIFU is based on the standard compressible Volume of Fluid (VoF) method. The transport equation of the liquid volume fraction is coupled with the continuity and momentum conservation equations to solve for the flow field.
Since the size of incipient bubbles formed by ultrasonically induced cavitation is generally smaller than the single cell, sub-grid models are used to describe nucleation, bubble dynamics and collapse unless the critical size of the bubbles or bubble cluster is enough to guarantee the creation of an interface. This last condition coincides with several adjacent cells having a volume fraction 0 (<1e-6). When a multi-cells bubble is created, the sub-grid models are de-activated, and the newly formed bubble is simulated with the compressible VoF method.
The nucleation was simulated by adopting an empirical correlation based on experimental evidence reported in several works. However, it is important to point out that developing a nucleation model to build a fully predictive numerical model to simulate HIFU is essential.
The Keller--Miksis (KM) equation described the bubbles' dynamics. This equation is derived by assuming spherical symmetry and applying the Navier--Stokes equations projected onto the radial coordinate.
Finally, the collapse was determined by a cavitation threshold that was, once again, derived from an empirical correlation based on experimental evidence as the available thresholds, such as the so-called “Blake threshold” are not suitable for the problem under study.
The vibration frequency and forcing pressure were used to determine the fluctuating pressure boundary condition for each transducer composing the transducer array used in the experiments. The numerical model was used to simulate several cases present in the literature.
This work presents the first step towards realising a predictive model for simulating ultrasonically induced cavitation in biological fluids. The framework was realised with the scope of evaluating bubbles' cloud location, size and cavitation intensity, thus allowing better treatment control.

***Keywords*:** Ultrasounds; Cavitation; CFD; Volume of Fluid (VoF)

1. Introduction

High Intensity Focused Ultrasounds (HIFU) treatment is a minimally invasive medical procedure which involves the use of ultrasounds to target alteration (and eventually destruction) of a specific tissue.

HIFU are used to treat a variety of conditions such as certain types of tumors, tremors and has applications in drug delivery.

The mechanism behind the effectiveness of HIFU is the induced high temperature, shear and eventual cavitation associated with focusing high frequency pressure waves in the region of space. Although HIFU are not an invasive technique, some side effects might limit their application [1]. Estimating the cavitation cloud's location, extension and intensity is paramount to minimising collateral damage. Computational modelling, therefore, has been adopted to optimize treatment strategies, design new HIFU probes and assess the collateral damage of the treatment. One aspect which has not been targeted by many authors is the description of bubbles’ formation within the liquid medium. The rapid variation in pressure in a confined space triggers the formation of gas pockets which form when the liquid is its metastable state.

The goal of this work is to model the formation of bubbles in a biological fluid as a first effort towards a predictive description of HIFU applications. The work starts with the presentation of the physical problem which is modelled by the Navier-Stokes equation solved for a multiphase mixture via the Volume of Fluid (VoF) method. The interface between liquid and gas is not geometrically reconstructed but assumed as a continuum in a framework typically named algebraic VoF.

A sub-grid model is adopted to simulate the dynamics of the oscillating bubbles. The sub-grid model is based on the Keller-Miksis 1-D Navier Stokes accounting for the viscoelasticity of the medium via the Voigt model [2].

Two applications of the model are presented, the first concerning cavitation ultrasound beam formation in water and the second concerning cavitation induced in an artery by applying an ultrasound source having a frequency of 0.5 MHz.

2. Numerical Model Description

The numerical model proposed in this work adopts the common Volume of Fluid (VoF) technique. The transport equation of the liquid volume fraction is coupled with the continuity and momentum conservation equations to solve for the flow field. Since the size of incipient bubbles is often much smaller than the computational domain, sub-grid models are used to describe nucleation, bubbles' dynamics and collapse. The Keller–Miksis equation was selected to describe the bubble dynamics in a non-Newtonian fluid. The bubble dynamics is solved in each computational cell and coupled to the flow field through source terms in the transport equations. The interface between bubbles and bulk flow is not fully resolved. Instead, a diffuse interface approach is used. A diffuse interface approach is justified because the solver must be efficient for real applications involving large computational domains. In the following, the components of the model are described in detail.

2.1 Bubble Sub-Models

UIC involves the dissipation of mechanical energy in a rather peculiar and unique way. The mechanical energy provided by the sonotrode, through high-frequency vibration, is converted for the nucleation and oscillation of the vapour bubbles. During the collapse, the energy stored in the bubble is released into a minimal volume, leading to local hot spots characterized by high pressure and temperature. Heat is transferred from the hot spots to the continuous phase leading to a temperature increase in the bulk liquid, which is lower by magnitude than the hot spots. The evolution of a bubble consists of three steps: nucleation, oscillation, and collapse.

Comprehending the complex phenomenon of nucleation is essential to building a physical model that accurately predicts the density and size of the vapour bubbles during ultrasonic cavitation. In the classical context of hydrodynamic cavitation, when the bulk pressure of the liquid goes below the saturated vapour pressure threshold, bubble nucleation may occur in discrete points of the fluid domain, and the cavitation intensity is a function of the bulk pressure and velocity of the flow field. This approach, however, is not suitable for system in which cavitation is induced by ultrasounds propagation as cavitation occurs while the liquid is in its metastable state. The approach adopted in the present work is described more deeply in [5] defines the domain of existence of the bubbles assuming a threshold of 1 MPa which is in agreement with the literature. Accordingly, in the present CFD code, the bubble inception as the onset of cavitation is triggered when the pressure amplitude within a computational cell exceeds the threshold. The bubbles density function is then described with the hyperbolic tangent function proposed by Vanhille [4] expressed as:

$$N = \begin{cases} N_{max} \tanh\left(\left|\dfrac{P - P_{Threshold}}{P_{Max} - P_{Threshold}}\right|\right) & \text{if} |P| \geq P_{Threshold}, \\ 0 & \text{if} |P| < P_{Threshold}, \end{cases}$$

where P_{Max} corresponds to the cavitation threshold of the medium that was proposed by Vanhille in his formulation [4], and N_{max} is the maximum bubble density that can be reached within the computational cell.

After the nucleation step, vapour bubbles oscillate at high frequency. The Keller–Miksis (KM) equation describes the bubbles' dynamics. This equation is derived by assuming spherical symmetry and applying the Navier–Stokes equations projected onto the radial coordinate. It is written in complete form as:

$$(1-c^{-1}\frac{dR}{dt})R\frac{d^2R}{dt^2}+\frac{3}{2}(1-3c^{-1}\frac{dR}{dt})\frac{dR^2}{dt}=\frac{P_a(t)-P(t)}{\rho_L}(1-c^{-1}\frac{dR}{dt})-\frac{R}{\rho c}\frac{d}{dt}(P_a(t)-P(t))$$

and P_a is calculated as:

$$P_a(t)=P_g-\frac{2\sigma}{R}+3\int_R^{\infty}\frac{\tau_{rr}}{r}dr$$

Here the shear stress τ_{rr} is defined as:

$$\tau_{rr}=G\gamma_{rr}+\mu\dot{\gamma}_{rr}$$

This differential equation expresses the bubble radius as a function of time (R) when the vapour bubble is subject to an external pressure field, $P(t)$. The properties of the fluid are ρ, μ and σ, respectively, the density, dynamic viscosity and surface tension of the liquid. These parameters depend strongly on the liquid temperature T, therefore requiring the KM equation to be solved together with the energy equation. The terms on the left-hand side represent the inertial contributions to momentum along the radial direction, while the terms on the right-hand side represent the instantaneous tension or driving force due to the pressure difference, and contributions of the kinematic viscosity and surface tension to the bubble dynamics. The shear stress is significant when dealing with viscoelastic materials. The Voigt model was used in this work according to what was done by Yang et al. [2] In the formulation of the shear stress, G is the shear modulus, γ_{rr} is the strain, and $\dot{\gamma}_{rr}$ is the strain rate.

Figure [1] shows that bubble oscillations and pressure fluctuations have two different time scales, which justifies the choice of de-coupling the flow field and the bubbles' dynamics in the numerical algorithm.

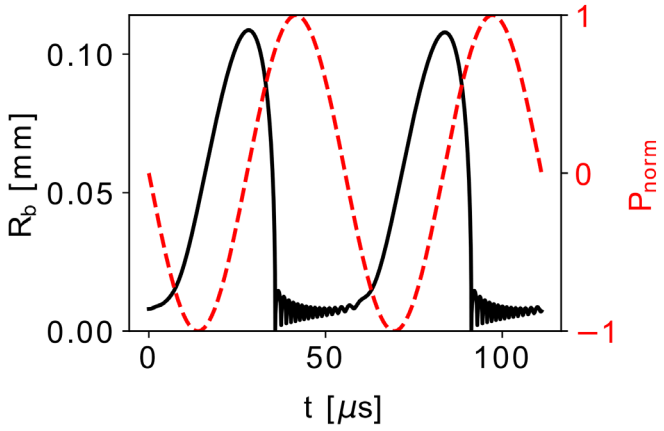

Figure 1 Solution of the KM equation describing a bubble oscillating because of an imposed sinusoidal pressure variation.

The KM equation is solved via a semi-implicit method with the time step set to be smaller than 1e-9 s. Following the domain of existence of bubbles proposed by Louisnard [3], the collapse of the bubbles is assumed to happen when the pressure amplitude falls below the Blake threshold pressure, which is the minimum pressure that guarantees the existence

of cavitation bubbles. The collapse is represented by simply assuming the instantaneous disappearance of gas bubbles and imposing the volume fraction of liquid equal to one. From a physical point of view, the energy stored in the oscillating bubbles is released in a tiny portion of space during the bubbles' collapse.

Note that interaction between bubbles is neglected as the dynamic cloud interaction parameter (B) is low for the cases considered . The latter is a function of bubbles number density (N_b), bubble radius (R_b) and cloud radius (R_{cloud}):

$$B = \frac{N_b R_b}{R_{cloud}},$$

where is the dimension of the bubbles' cloud, generally 3-4 orders of magnitude larger than the bubbles' average radius for the cases studied.

2.2 Flow Modeling

An Eulerian volume-of-fluid (VoF) method is adopted to model the two-phase flow, describing the dynamics of two-phase compressible fluids with a unified velocity **u**, pressure P, and temperature T. In the following, the computational domain is defined as $\Omega \in R^3$ while the two subsets Ω_1 and Ω_2 represent the liquid and gas phase, respectively. The intersection of the two subsets is the interface $\Gamma \in R^2$. The interface Γ can be seen as the boundary between two adjacent phases, Ω_1 and Ω_2 . A phase indicator function captures the evolution of the interface:

$$f(\mathrm{x}, t) = \begin{cases} 1 & x \in \Omega_1(t), \\ 0 & x \notin \Omega_2(t), \end{cases}$$

Referring to the liquid phase and indicated with Ω_1. The next step is discretizing the computational domain by dividing it into a discrete number of control volumes (computational cells) C_l for $C_l = l = 1, .., N_c$.

In the context of a finite volume representation, at a given time, the variable determines the volume fraction of liquid in a given computational cell:

$$\alpha_l(t) \equiv \frac{1}{V_l} \int_{C_l} f(\mathrm{x}, t) dV\,,$$

where V_l is the control volume of the l-th cell, note that the liquid volume fraction is a continuous variable, although it is defined as a cell-averaged quantity. The liquid volume fraction, therefore, takes on the value:

$$\alpha(\mathrm{x}, t) = \begin{cases} 1 & \text{within the liquid,} \\ ]0,1[& \text{at the interface,} \\ 0 & \text{within the gas.} \end{cases}$$

For consistency, α is defined as the liquid volume fraction, while $1 - \alpha$ is the gas volume fraction. All local physical quantities are calculated as a linear combination of the properties of the two phases. The local quantity in the liquid and gas phase also depends, in general, on the composition of the mixture. A general physical property ψ is then expressed as:

$$\psi = \alpha\psi_1 + (1 - \alpha)\psi_2,$$

The transport equation for the volume fraction of a compressible fluid experiencing phase change is expressed as

$$\frac{\partial(\alpha\rho)}{\partial t} + \nabla \cdot (\alpha\rho\mathbf{u}) = -\dot{m}\delta_{\Gamma},$$

where is the mass exchange rate due to phase change across the interface and is the surface area density at the interface which is given by the surface of the bubbles present in the computational cell. The mass exchange flux contribution has a negative sign if the liquid evaporates and a positive sign if the vapour condenses. On the other hand, the mass and momentum conservation equations describe the bulk fluid motion, noting that the incompressibility assumption does not hold in the bubble bursts because of the high velocities resulting from severe pressure gradients within the droplet. The continuity and momentum equations are expressed, respectively, as follows:

$$\frac{\partial\rho}{\partial t} + \nabla \cdot (\rho\mathbf{u}) = 0,$$

$$\frac{\partial(\rho\mathbf{u})}{\partial t} + \nabla \cdot (\rho\mathbf{u}\mathbf{u}) = \nabla \cdot [\mu(\nabla\mathbf{u} + \nabla\mathbf{u}^T)] - \nabla P + \mathbf{f}_s + \rho\mathbf{g},$$

where g represents the gravitational acceleration, μ is the dynamic viscosity, and $\mathbf{f}_s$ is the surface tension force.

The surface tension force $\mathbf{f}_s$ is important and generally modelled with the continuum surface force (CSF) method, introduced in reference:

$$\mathbf{f}_s = \sigma q \mathbf{n},$$

where σ is the surface tension coefficient, $\mathbf{n}$ is the unit normal vector to the interface and q is the curvature, expressed as the divergence of the normalized gradient of the volume fraction:

$$q = -\nabla \cdot \left(\frac{\nabla\alpha}{|\nabla\alpha|}\right)$$

Finally, the energy equation is also solved to determine the liquid temperature:

$$\frac{\partial(\rho c_p T)}{\partial t} + \nabla \cdot (\rho c_p \mathbf{u} T) = \nabla \cdot (k\nabla T) - \dot{\mathrm{m}}\Delta H_v,$$

where the last term describes the enthalpy of vaporization exchanged because of the eventual phase change, k is the thermal conductivity, c_p is the heat capacity at constant pressure, and ΔH_v is the heat of vaporization. The energy equation formulation above neglects the terms associated with pressure and viscous stresses, which are typically small.
By solving the KM equation, the source term $\dot{m}$ is calculated as:

$$\dot{m} = 4\alpha_2 \frac{\rho_1\rho_2}{\rho R}\frac{dR}{dt},$$

R is the average radius of the bubbles present in the individual cells, the source term is then included in the volume fraction equation. An operator-splitting approach is employed in its solution procedure.

Solving the momentum equation starts from considering the following linearization:

$$\frac{\rho^*\mathbf{u}^{n+1} - \rho^n\mathbf{u}^n}{\Delta t} + \nabla \cdot (\rho\mathbf{u}^*\mathbf{u}^{n+1}) = \nabla \cdot (\mu(\mathbf{u}^*\nabla + \nabla(\mathbf{u}^*)^T)) - \nabla P^{n+1} + \mathbf{f}_s + \nabla(\rho^*)\mathrm{g} \cdot \mathrm{x}$$

The momentum equation is then discretized as:

$$\mathcal{M}\mathbf{u} = -\nabla P + \mathbf{f}_s + \nabla(\rho)\mathrm{g}\cdot\mathbf{x},$$

where $\mathcal{M}$ is the coefficients matrix of the velocity vector. The coefficients matrix is further decomposed, resulting in the following formulation:

$$\mathcal{A}\mathbf{u}^{n+1} = \mathcal{H}(\mathbf{u}^*) - \nabla P^{n+1} + \mathbf{f}_s + \nabla(\rho^*)\mathrm{g}\cdot\mathbf{x},$$

where $\mathcal{A}$ and $\mathcal{H}$ represent the diagonal and off-diagonal terms of the coefficients matrix, the superscript denotes the provisional values of the variables in the iterative solution procedure.
The pressure equation is derived from the conservation of momentum and volume fraction of the liquid, resulting, after linearization, in the following:

$$\left(\frac{\alpha_1^*}{\rho_1^*}\frac{\partial\rho_1^*}{\partial P_{tot}} + \frac{\alpha_2^*}{\rho_2^*}\frac{\partial\rho_2^*}{\partial P_{tot}}\right)\left(\frac{P_{tot}^{n+1} - P_{tot}^{n}}{\Delta t} + \mathbf{u}^*\cdot\nabla P_{tot}^{n+1}\right) + \nabla\cdot\mathbf{u}^{n+1} - \dot{m}^*\left(\frac{1}{\rho_1^*} - \frac{1}{\rho_2^*}\right)\delta_\Gamma = 0$$

The pressure equation is solved implicitly after an additional linearization step. For the cases considered in this work, the discretized transport equations were solved using the PIMPLE method, which combines the Pressure Implicit with

Splitting of Operators (PISO) and Semi-Implicit Method for Pressure Linked Equations (SIMPLE) iterative procedures. The momentum and pressure equations are solved sequentially until convergence is achieved. In particular, the Geometric Agglomerated Algebraic Multigrid (GAMG) strategy was utilized to solve the pressure equation.

A second-order Gauss linear reconstruction was employed for the spatial discretization, except for the convective terms of the volume fraction and momentum equations. The newly developed solver was implemented in the OpenFOAM v2023 framework. The main steps of the solution procedure are listed in the following algorithm:

The newly developed solver was implemented in the OpenFOAM v2306 framework. The main steps of the solution procedure are listed in the following algorithm:

```
while t < t_end do
    Solve α equation;
    Solve α evaporation equation;
    for i ← cell_0 to cell_N do
        if |P[cell_i]| > |P_Threshold[cell_i]| then
            if α[cell_i]=0 then
                Obtain equilibrium radius and nucleation rate;
            else
                Solve Keller–Miksis equation;
                Obtain instantaneous radius and radius rate of change;
                if R<R_Blake then
                    Impose α[cell_i]=0 and calculate energy source term;
                end
            end
        end
    end
    Solve Energy equation;
    Solve Pressure-Velocity coupling;
    Update mesh, check and correct mass conservation;
end
```

Figure 2 Algorithm of the numerical solver.

3. Discussion

The solver was used to simulate two cases. The first case was an attempt at replicating an experiment presented in the the work of [6]. The mesh is reported in Figure 3 on the left while a snapshot from the numerical simulation results is reported on the right. The figure illustrates the beam formation because of the propagation of the pressure waves. The system is simulated by imposing a sinusoidal boundary condition for the pressure having a maximum amplitude of 0.5 MHz. The cell size at the focal point is approximately 10 μm x 10 μm x 10 μm while in the rest of the domain it scales until it reaches 1 mm. The second application consisted of a numerical simulation of cavitation induced with the same system in a blood vessel (Figure 4). The blood vessel was simulated by simply changing the physical properties of the liquid in the region identified by its presence. It is possible to notice how the bubbles form preferentially on the surface of the vessel.

4. Conclusions

This work presents the first step towards realising a predictive model for simulating ultrasonically induced cavitation in biological fluids. The framework was realized with the scope of evaluating bubbles' cloud location, size and cavitation intensity, thus allowing full control of the treatment. Two major approximations are associated with this model: the assumption of a cavitation threshold and a nucleation rate. In fact, the model totally depends on how many bubbles we allow to form within the computational domain, defeating the purpose of creating a predictive framework. Another limitation of this model is that it does not allow to estimate damage on a given tissue since the jet formation can't be resolved with the resolution adopted in this work. The future development will target the introduction of two distinct areas in the computational domain, the first, aimed at waves propagation and the second aimed at accurately simulate cavitation at a much smaller scale.

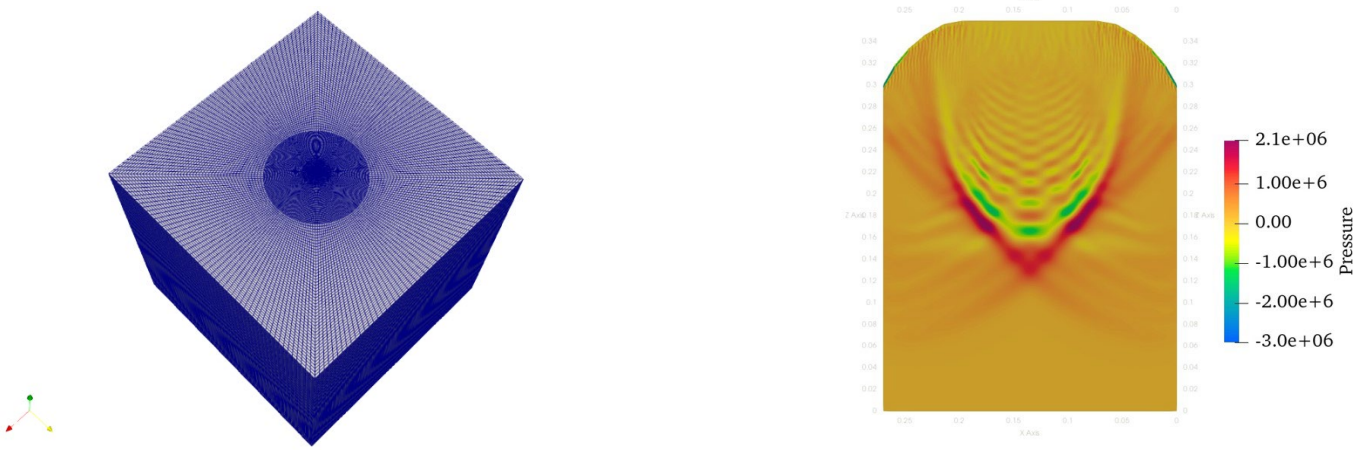

Figure 3 On the left a 3D view of the computational domain. The circular region on top represents the discretized transducer. On the right a snapshot for the simulation. It is possible to clearly observe the structure of the ultrasound beam.

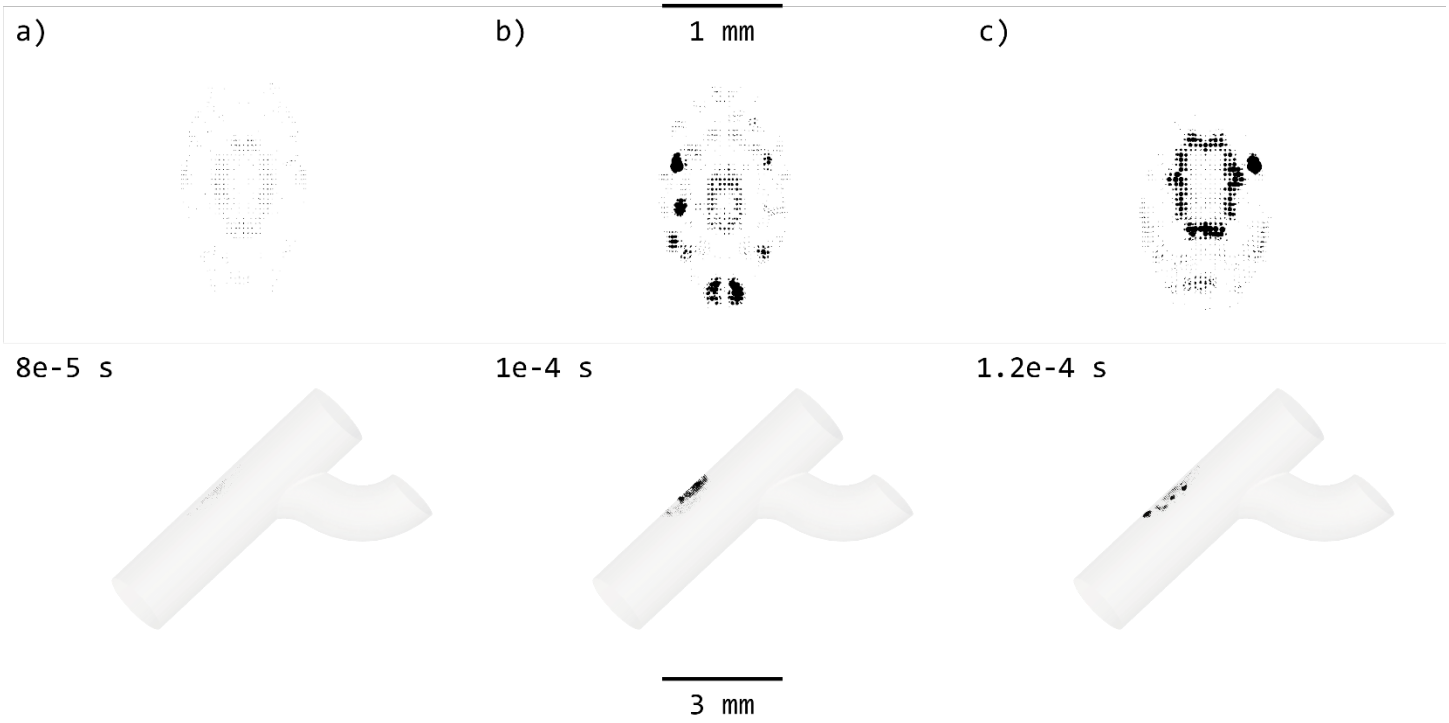

Figure 4 Numerical simulation of UIC induced in a blood vessel by applying an ultrasonic force at a frequency of 1 MHz with a driving pressure of 1MPa. Figure a), b) and c) show three different steps in the cavitation process. The upper pictures illustrate an orthogonal view of the cavitation cloud, while the bottom pictures show the entire domain. The cloud is visualized by creating spheres having a volume $V = (1 - \alpha)V_{cell}$.

Acknowledgements

This work was sponsored by King Abdullah University of Science and Technology (KAUST).

References

[1] Xu, Z., Hall, T.L., Vlaisavljevich, E. and Lee Jr, F.T., Histotripsy: the first noninvasive, non-ionizing, non-thermal ablation technique based on ultrasound. *International Journal of Hyperthermia*, 2021, *38*(1), pp.561-575.

[2] Yang, X. and Church, C.C., A model for the dynamics of gas bubbles in soft tissue. The Journal of the Acoustical Society of America, 2005, 118(6), pp.3595-3606.

[3] Louisnard, O., A simple model of ultrasound propagation in a cavitating liquid. Part I: Theory, nonlinear attenuation and traveling wave generation. 2012. *Ultrasonics sonochemistry*, *19*(1), pp.56-65.

[4] Vanhille, C., Numerical simulations of stable cavitation bubble generation and primary Bjerknes forces in a three-dimensional nonlinear phased array focused ultrasound field. 2020. *Ultrasonics sonochemistry*, *63*, p.104972.

[5] Guida, P., Viciconte, G., Ceschin, A., Colleoni, E., Pérez, F.E.H., Saxena, S., Im, H.G. and Roberts, W.L., Numerical model of an ultrasonically induced cavitation reactor and application to heavy oil processing. 2022. *Chemical Engineering Journal Advances*, *12*, p.100362.

[6] Macoskey, J.J., Hall, T.L., Sukovich, J.R., Choi, S.W., Ives, K., Johnsen, E., Cain, C.A. and Xu, Z., Soft-tissue aberration correction for histotripsy. *IEEE transactions on ultrasonics, ferroelectrics, and frequency control*, 2018. *65*(11), pp.2073-2085.